

PAPER • OPEN ACCESS

## A CFD/experimental comparative database to feed a predictive model for ground vortex characteristics

To cite this article: F Dupuy *et al* 2022 *IOP Conf. Ser.: Mater. Sci. Eng.* **1226** 012011

View the [article online](#) for updates and enhancements.

You may also like

- [Simulation Study of the Effect of Anti-Icing on the Nacelle Lip-skin Material](#)  
M H Y Syed, M A Ismail, Q Azam et al.
- [Driving Torque Control for a Nacelle Test Bench](#)  
Uwe Jassmann, Matthias Reiter and Dirk Abel
- [Investigation of the nacelle blockage effect for a downwind turbine](#)  
Benjamin Anderson, Emmanuel Branlard, Ganesh Vijayakumar et al.



The Electrochemical Society  
Advancing solid state & electrochemical science & technology

242nd ECS Meeting

Oct 9 – 13, 2022 • Atlanta, GA, US

Abstract submission deadline: **April 8, 2022**

Connect. Engage. Champion. Empower. Accelerate.

**MOVE SCIENCE FORWARD**



Submit your abstract



# A CFD/experimental comparative database to feed a predictive model for ground vortex characteristics

F Dupuy<sup>1</sup>, R Mendonça E Costa<sup>1</sup>, S Raynal<sup>1</sup>, V Camenen<sup>1</sup>, J-P Bouchet<sup>2</sup>, S Courtine<sup>2</sup>

<sup>1</sup>Capgemini Engineering, 4 Avenue Didier Daurat, 31700 BLAGNAC, FRANCE

<sup>2</sup>CSTB, 11 rue Henri Picherit – BP82341, 44323 NANTES Cedex 3, FRANCE

[fabien.dupuy@capgemini.com](mailto:fabien.dupuy@capgemini.com)

**Abstract.** Most modern aircraft engines rely on the use of high Bypass Ratios (BPR) turbofans to achieve both high thrust and low specific fuel consumption. However, such configurations are prone to the formation of ground vortices during low-speed operations. This phenomenon arises under specific combinations of wind direction, velocity or inlet air speed, generating engine vibrations and leading to the suction of damaging abrasive particles. Its characterization in early design stages is crucial. In this work, a joint experimental and numerical exploration of operating conditions leading to ground vortex presence is carried out on a scaled wind tunnel configuration. Flow details are investigated for several working points obtained from a specific set of input parameters (intake speed, wind speed, ground clearance). A methodology suitable for both experimental and Computational Fluid Dynamics (CFD) works is developed to extract vortex characteristic quantities, based on a local pressure minimum and Q-criterion contours topology. A very good agreement is obtained when comparing vortex predictions stemming from CFD and experiments. This database shall be used to transpose experimental data probed outside of the nacelle to data within the nacelle using data analytics techniques, paving the way for future data driven predictive models.

## 1. Introduction

The aircraft transportation industry is often identified as one of the major greenhouse gas and pollution creators in the general opinion, although considerable efforts have been made over the last decades. Increasingly stringent regulations have pushed engine manufacturers to develop better designs that would allow for lower specific fuel consumption. Among other means, this can be achieved by using high Bypass Ratio (BPR) turbofans for which most of the intake air is routed around the turbine. High BPR designs are used by most common civil airliners and have resulted in larger engine nacelles [1], and thus reduced clearance between the casing and the ground. Note that so-called “open-rotor” configurations are also scrutinized for future aircrafts [2]. Reducing ground clearance however facilitates the development of vortical structures originating from the soil and being sucked into the lower part of the fan during stationary or low-speed airport manoeuvres. Ground vortices can lead to the ingestion of foreign objects that could damage fan blades [3, 4], total pressure distortion leading to an imbalanced fan load, or vibrations [5, 6]. They can be created under either headwind or crosswind conditions, with stronger vortices observed in the latter case according to [7]. Identifying the occurrence of such phenomena during early engine conception phases is therefore crucial.



Previous studies in the literature have identified the key role of the engine speed, wind speed and ground clearance height as determining conditions leading to the apparition of this phenomenon on reduced scale configurations by means of experiments [7, 8], or numerical simulation [4]. Predictive ground vortex tools are however still not widely used, and expensive full scale engines tests need to be carried out

The present study focuses on the analysis of vortex formation and ingestion by aircraft engines in ground operations under crosswind conditions. The framework of this investigation is the InVIGO project, part of the CleanSky 2 initiative and funded by European Union's Horizon 2020 research and innovation programme (under grant agreement no. 864288). The project combines Wind Tunnel (WT) test results with CFD numerical simulations performed in the WT geometry to provide a comprehensive characterization of vortex ingestion and a rich database to develop a predictive model for vortex characteristics using data analytics. In particular, CFD is used to transpose experimental data probed outside of the nacelle into fan plane information.

The paper first describes both experimental and CFD scaled setups that have been used throughout this work. A following part presents the methodology used to extract ground vortex positions and characteristics. Finally, a comparison of the experimental/CFD databases and results are presented.

## 2. WT test campaigns

### 2.1. WT configuration/setup

Experimental measurements were carried out on a reduced scaled version (1/6.5) of a Safran nacelle without fan blades or rotating parts, and a characteristic diameter  $D$  not disclosed for confidentiality reasons. Variations of the average intake speed  $U_i$  within the nacelle were achieved using a large centrifugal varying-speed fan connected to the nacelle via an aeraulic duct of about 20 m.  $U_i$  was estimated in the fan plane (spinner cross-section omitted) from ambient conditions and engine mass flow rate using isentropic calculations. The whole setup was operated within CSTB's Jules Verne wind tunnel, at atmospheric temperature and pressure conditions. The test section is 6x5x12m, with adjustable wind speed  $U_\infty$ . Hence, the reduced speed  $U^* = U_i/U_\infty$  could be varied between 2 to 37. The nacelle was positioned above a table representing the ground. Its height  $H$  could be adjusted to control the ground clearance ratio  $H/D$ . Seven ratios were studied, between about 0.8 to 1.5. Figure 1 illustrates the testing apparatus.

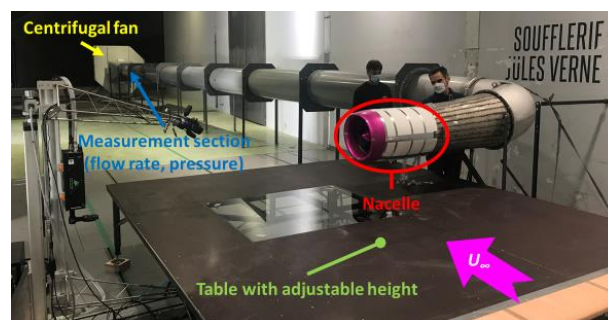


**Figure 1.** Test setup used during experimental campaigns within the Jules Verne wind tunnel.

### 2.2. Measurement techniques and data acquisition

The inlet lip was equipped with about 80 irregularly distributed pressure taps (see Figure 2.a), with more pressure taps on the upwind side (windward side). The inlet was also equipped with an instrumented shell with 8 pressure rakes regularly distributed around the air intake, with 7 total pressure measurements on each rake (Figure 2.b). All pressure taps and rakes were connected to KULITE differential pressure sensors (KMPS type) located at the back of the model via vinyl tubes. Three different sensors' ranges,

whose distribution were adjusted by preliminary CFD calculations, were used:  $\pm 7$  kPa,  $\pm 35$  kPa and  $\pm 50$  kPa. The acquisition was carried out over a period of at least 80 s, with a frequency of about 125 Hz.

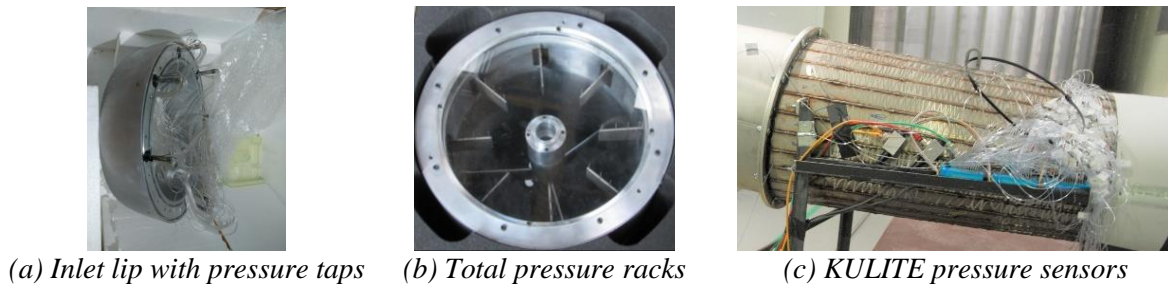


**Figure 2.** Inlet lip with pressure taps and total pressure rakes instrumented with KULITE sensors.

Stereo-PIV measurements were also involved. A LaVision system was used, consisting of 2 Imager SX6M Cameras (6 Mpixels), and an Evergreen Laser (200mJ / pulse). The system was positioned on a 2 axes robot. Seeding was done with oil droplets ( $\sim 1\mu\text{m}$  diameter). The Stereo-PIV (S-PIV) was implemented to characterize velocity fields in 3 measurement planes: 2 horizontal planes (see Figure 3.a) and 1 vertical plane (see Figure 3.b). Those measurement planes were located in the vicinity of the nacelle or the ground in order to obtain vortex characteristics as close as possible to the inlet entrance. 1000 vector fields were recorded during 80 s for each test configuration, with a 12.5 Hz sampling frequency. S-PIV measurements were concomitant with the pressure acquisitions previously described.

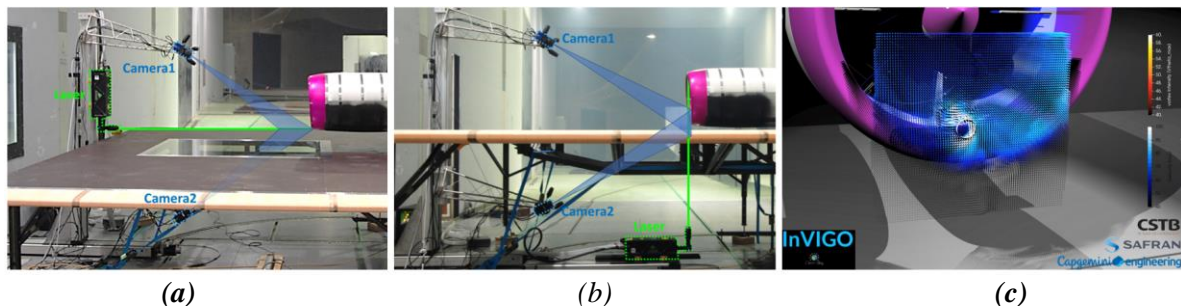


**Figure 3.** S-PIV measurements planes setup (a and b). Example of instantaneous velocity field obtained from S-PIV on the vertical plane (c).

### 2.3. Treatment of experimental results

From total pressure measurements, it was possible to assess distortion indices. Pressure values recorded in the fan section will eventually be used as input for the final predictive model, which is the main focus of the InVIGO project. For S-PIV calculations, the cross-correlation window was progressively reduced to reach a final size of  $64 \times 64$  pixels with 50% overlap. The resulting spatial resolution of the velocity fields is about 3 mm. For each plane, the 3 components of the velocity field were obtained. An example of instantaneous velocity field obtained is illustrated on Figure 3.c. Ground vortices are also identified according to the procedure described in § 4.1.

## 3. CFD Physics and numerical setup

### 3.1. Geometry and mesh

The computational domain was modelled after the real testing facilities dimensions used during experimental measurement campaigns described in the previous section and is shown in Figure 4.

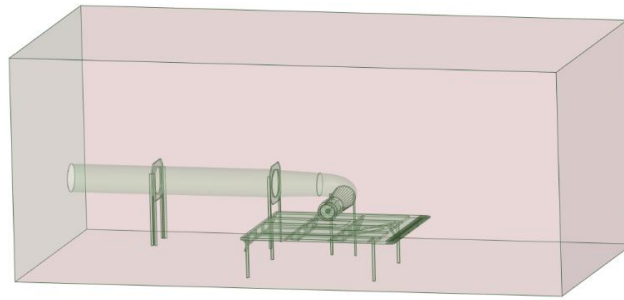


**Figure 4.** Simplified geometry used in CFD simulations.

The CAD geometry was slightly simplified to accommodate the meshing process. Namely, fine pipeline elements and pressure rakes within the intake were removed, as well as the PIV camera system. Note that prior tests on few configurations with these elements included only showed marginal differences with the proposed setup. Unstructured meshes featured 59 to 63 million cells depending on the considered ground clearance  $H/D$ . Most of the domain was meshed with tetrahedral cells while near walls regions also included prisms layers to reach dimensionless wall distances  $y^+ < 3$  in order to fully resolve the viscous sublayer.

### 3.2. Numerical formulation

Simulations were carried out using the commercial code Ansys Fluent. Unsteady computations were carried out under the URANS formalism with the Scale Adaptive Simulations (SAS) method combined with a  $k\omega - SST$  turbulence model for closure. This ensures a fine resolution of transient phenomena in regions of interest while maintaining an unsteady RANS description in coarse areas of the grid (where small turbulence scales are not captured). Unsteady simulations were crucial for an accurate determination of the quantities of interest, namely, for an analysis of selected variables over time, and for the calculation of associated statistics (minimum, maximum, or RMS values, for example). Initialization relied on steady (RANS) calculations, following guidelines determined during the previous stages of the project [9]. For the unsteady part of the calculations (SAS), the strategy also relied deeply on previous knowledge obtained from earlier calculations in the context of the project [9]. A coupled scheme was used to handle the pressure-velocity coupling and a classical value of  $10^5$  was chosen for the Courant number, with a time step  $dt = 10^{-4}$ s. The extraction of reference plane data was performed periodically during the last 180 ms of flow time simulation, resulting in 400 temporal snapshots. Longer simulation times could not be handled due to the large number of configurations to be tested and computational power constraints.

### 3.3. Ground vortex: quantities of interest

For CFD simulations, three planes of interest are considered (Figure 5). The first two correspond to the vertical and horizontal PIV planes used in experiments. The fan plane is located at a distance  $l_d$  from the vertical PIV plane (few centimetres), within the nacelle. It corresponds to the location of fan blades in the full-scale engine and is the primary zone of interest for ground vortex characterisation. For engine manufacturers, the prediction of vortex related quantities should ideally be made directly on the fan plane. For this reason, 42 configurations were simulated using CFD, with 24 common reference configurations corresponding to cases with available experimental data. They correspond to a large range of intake velocity, wind speed and elevation representative of actual aircraft nacelle ground operations.

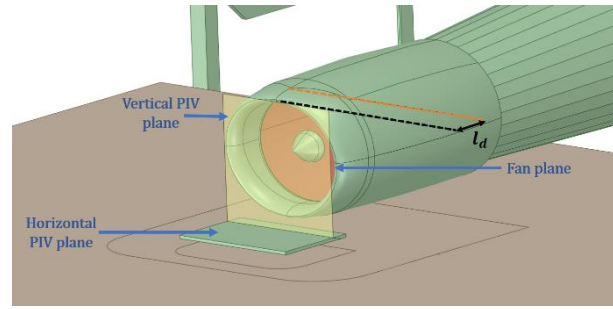


**Figure 5.** CAD representation of the planes of interest for this study. Dimensions have been modified for confidentiality purposes.

The objective of running concurrent CFD simulations is to build a transfer function between vertical PIV plane data and fan plane data. Thus, experimental data could be used directly to infer fan plane vortex features. For the present study, the so-called vortex characteristics are given in Table 1.

**Table 1.** Definition of vortex characteristics of interest

Quantity	Definition	Unit
$r_c$	Vortex center radius: distance from the spinner axis on the fan plane	[m]
$\theta_c$	Vortex center angle: angle with the vertical axis (positive in the wind direction)	[°]
$R_{eq}$	Vortex tube equivalent radius, if assumed to be cylindrical	[m]
$\Gamma$	Vortex strength (circulation)	[m <sup>2</sup> .s <sup>-1</sup> ]
$v_\theta$	Vortex tube tangential velocity	[m.s <sup>-1</sup> ]

## 4. Results

### 4.1. Post-processing strategy for vortex characteristics

The identification of vortices and coherent structures has been a long-debated topic in fluid dynamics [11]. For intake vortices, distortion indices based on pressure averaging on portions of a disk have been fairly used in the literature [9, 12]. While appealing from a theoretical standpoint, such quantities only provide a rough vortex position estimation if the angular sector is too large and fall back to a total pressure minimum determination if the sector is too narrow.

In this work, a local static pressure minimum, or vorticity maximum proved to be the most robust option for vortex centre identification. Once  $r_c$  and  $\theta_c$  are known, the Q-criterion [11] is used to identify the vortex topology on a given plane. This well-known quantity (hereafter noted  $Q$ ) is derived from the matrix norm difference between the symmetric and anti-symmetric parts of the velocity gradient tensor,  $S_u$  and  $\Omega_u$ :

$$Q = \frac{1}{2} (\|\Omega_u\|^2 - \|S_u\|^2) \quad (1)$$

A total of 31 contours encompassing the identified vortex centre is computed. For each contour, the vortex circulation  $\Gamma$  is computed from the vorticity surface integral according to Stokes's theorem using the surface  $S$  contained within the Q-criterion contour and the vorticity  $\omega$  normal to the plane considered. The equivalent radius  $R_{eq}$  and tangential velocity  $v_\theta$  can then be inferred using the formulas presented in Figure 6. The contour  $C$  maximizing the tangential velocity  $v_\theta$  is kept as the relevant one for vortex characteristics assessment.

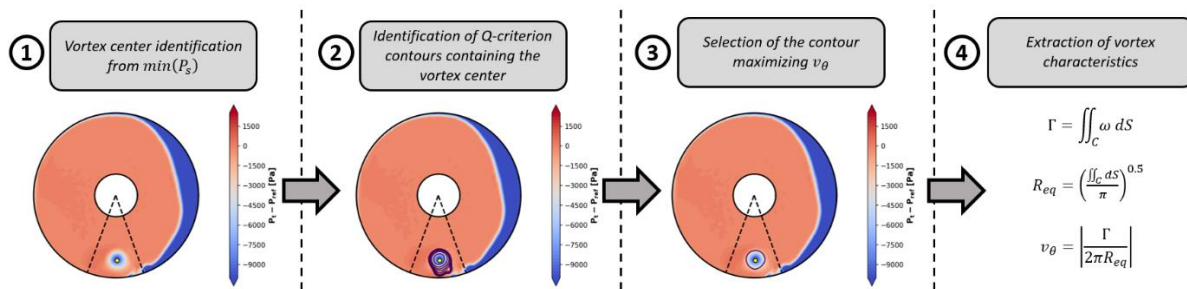


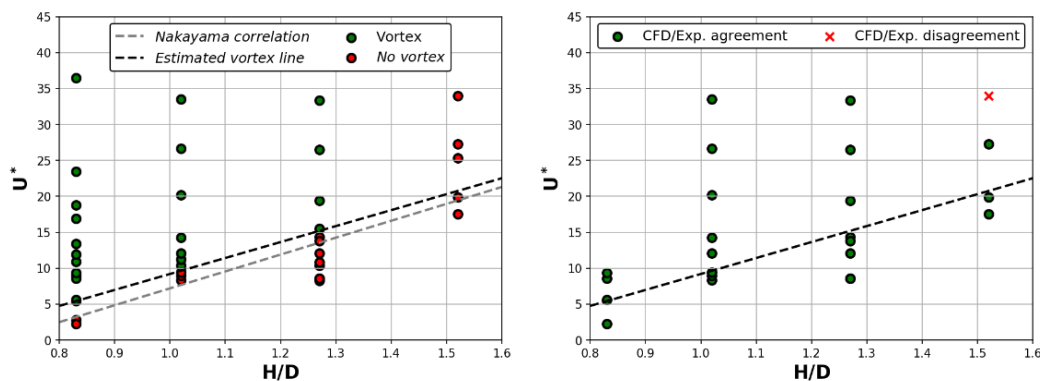
**Figure 6.** Schematic representation of the vortex identification methodology on the fan plane. The angular region around the mean predicted vortex centre is identified with the two dotted black lines.

The method can be indistinctly applied to experimental or CFD data. If the average position  $(r_c, \theta_c)$  of the vortex is known, the search for instantaneous vortex centers can be limited to an angular portion of the plane of interest, which avoids spurious center identifications when the adverse pressure gradient zone generated by the crosswind is large. The working principle of the algorithm is illustrated in Figure 6.

For each characteristic quantity, its average and RMS values are computed over the simulation time for CFD simulations, or over the acquisition time for experiments.

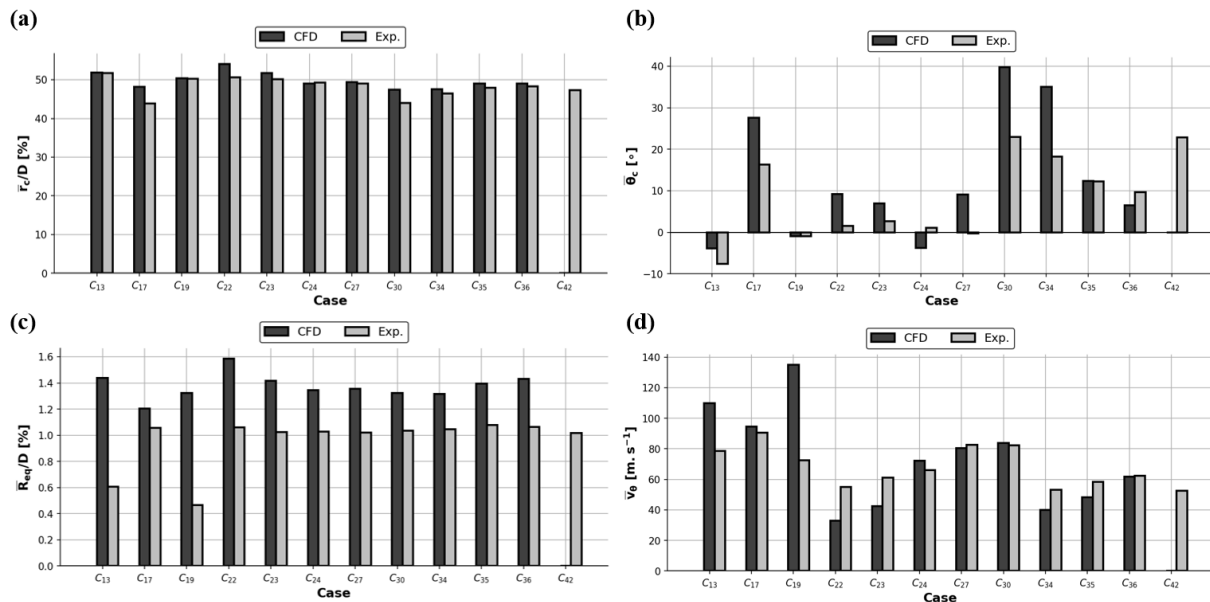
#### 4.2. Comparison between WT and CFD data

Figure 7 presents the 42 CFD cases results obtained in terms of vortex prediction after the first WT campaign. As previously mentioned, experimental data was also available for 24 of these cases. CFD and WT measurements are in agreement regarding the presence/absence of an intake vortex for 23 out of the 24 cases. The only outlier is a case with a high elevation  $H/D = 1.52$  and high  $U^*$  (hereafter noted case  $C_{42}$ ), which constitutes one of the most challenging case for the present URANS simulations. Indeed, tracking a coherent structure was not possible in this case. Among the 24 common configurations, 12 exhibited a strong coherent intake vortex according to WT data, compared to 11 according to CFD data which did not show a coherent structure for case  $C_{42}$ . The estimated vortex line is also drawn, although according to the data, a simple line may not be sufficient to accurately bound the vortex presence zone.



**Figure 7.** CFD simulated configurations on the  $H/D$  and  $U^*$  plane (left). The theoretical line of [10] and the separation line estimated from experimental data are also drawn. Agreement between CFD and experimental results on the 24 selected cases (right).

Following the post-processing strategy detailed in the previous section, vortex characteristics are gauged from both CFD and experimental fields on the vertical PIV plane. Figure 8.a,b shows the comparison of average vortex centre coordinates ( $r_c, \theta_c$ , cylindrical frame tied to the spinner) probed in the vertical PIV plane for the 12 cases exhibiting an intake vortex. Radial vortex positions predicted from CFD and WT data are in good agreement, while angular positions are also qualitatively predicted by numerical simulations.



**Figure 8.** Comparison of average radial vortex position (a), average vortex angle ((b),  $\theta_c = 0$ : vertical direction,  $\theta_c > 0$  in the wind direction), average equivalent radius (c) and average tangential velocity (d) on the vertical PIV plane obtained from CFD and WT data.

Figure 8.c,d displays the comparison of average equivalent radii and tangential velocities for the same subset of 12 cases. Equivalent radii are of the same order of magnitude for both data sources, although numerical computations seem to consistently overestimate values compared to WT data. Tangential velocities are in overall fair agreement except for cases  $C_{13}$  and  $C_{19}$  for which accurate velocity measurements could not be achieved using S-PIV in the vortex central core region. It is fair to say that despite a quantitative agreement, differences are still present. One may argue that some of the registered discrepancies could be explained by uncertainties in PIV measurements. Another explanation lies in the fact that the vertical PIV plane spatial discretization was not identical between CFD and experiments and may have been insufficient to yield perfectly reliable velocity gradients (and thus Q-criterion contours). Additionally, numerical data acquisition was performed during 180 ms with a sampling frequency  $f_s=2000$  Hz while WT data was acquired during several seconds with a sampling frequency  $f_s=12.5$  Hz. Hence, low frequency oscillations could not be captured with RANS simulations, and RMS quantities, not shown here for the sake of brevity, considerably differ. The impact of the discretization error could be quantified by performing a grid refinement study, while running longer simulations could alleviate the acquisition time differences. Nevertheless, the overall agreement is considered to be satisfactory given the project time frame and computational constraints.

## 5. Conclusion

The present work provided both numerical and experimental insights on intake ground vortices on a reduced-scale engine nacelle. It constitutes the first step towards building a database of cases that would feed a vortex predictive model based on data analytics. A robust post-processing methodology based on a local static pressure minimum and contours of Q-criterion was devised to compare data from both

approaches with the same exact procedure. CFD and WT experiments predicted the same occurrence of an intake vortex for a given ground elevation, wind speed and intake velocity triplet in almost all cases, proving the reliability of numerical methods for this application. Vortex characteristics were assessed and compared using both approaches on a series of reference planes, showing an overall fair agreement. In future works, CFD data will be used to build a transfer function between the vertical plane corresponding to the location of PIV measurements and the fan plane where vortex features need to be determined. The aim is to be able to fully use WT gauged data together with already valuable CFD data in an effort to build a database of vortex characteristics. Such a database shall be used as an input for data driven methods to build intake vortex prediction numerical tools relying on limited pressure measurements.

## Acknowledgments

The authors would like to acknowledge the support of Safran Aircraft Engines for this study. The InVIGO project has received funding from the Clean Sky 2 Joint Undertaking under the European Union's Horizon 2020 research and innovation programme under grant agreement n°864288. This communication and the data provided here represent only the author's view and do not engage CleanSky 2 nor the European Union for any use that may be made of the information they contain.

## References

- [1] Magrini A, Benini E, Yao HD, Postma J and Sheaf C 2020 A review of installation effects of ultra-high bypass ratio engines *Progress in Aerospace Sciences* **119** 100680
- [2] Hendricks E and Tong M 2012 Performance and weight estimates for an advanced open rotor engine *48th AIAA/ASME/SAE/ASEE Joint Propulsion Conference & Exhibition* 3911
- [3] Rodert Lewis A and Garrett FB 1955 *Ingestion of foreign objects into turbine engines by vortices*.
- [4] MacManus DG and Slaby M 2015 Intake ground vortex and computational modelling of foreign object ingestion *The Aeronautical Journal* **119** 1123-1145
- [5] Motycka DL 1976 Ground Vortex-limit to Engine-reverser Operation *ASME J. Eng. Power* 258-263
- [6] Green JS 2008 Force response of a large civil fan assembly *Turbo Expo: Power for Land, Sea and Air* **43154** 685-692
- [7] Murphy J and Macmanus DG 2011 Ground vortex aerodynamics under crosswind conditions *Experiments in Fluids* **50** 109-124
- [8] Murphy J and Macmanus DG 2011 Inlet ground vortex aerodynamics under headwind conditions *Aerospace Science and Technology* **15** 207-215
- [9] Mendonça e Costa R, Millot G, Raynal S, Bouchet JP and Courtine S 2021 Unsteady simulation of intake ground vortex ingestion in real wind tunnel conditions *55<sup>th</sup> 3AF International Conference on Applied Aerodynamics*.
- [10] Nakayama A and Jones JR 1999 Correlation for formation of inlet vortex *AIAA Journal* **37** 508-510.
- [11] Jeong J and Hussain F 1995 On the identification of a vortex *J. Fluid Mech* **285** 69-94.
- [12] Murphy J 2008 *Intake ground vortex aerodynamics* (Cranfield University).
- [13] Berthelon T, Dugeai A, Langridge J and Thouverez F 2019 Analysis of vortex ingestion impact on the dynamic response of the fan in resonance condition *Turbo Expo: Power for Land, Sea and Air* V07AT36A010.
- [14] Zantopp S, MacManus DG and Murphy J 2010 Computational and experimental study of intake ground vortices *The Aeronautical Journal* **114** 769-784